Supporting Information for

Modulating 2D Heterointerface with g-C_3N_4 Meshes: A Suitable Hetero-Layered Architecture for High-Power and Long-Life Energy Storage

Yunping Wu, Wei Wei, Tianyi Ding, Sheng Chen, Rui Zhai and Caihe Bai*

Department of Applied Chemistry, School of Chemistry, Xi'an Key Laboratory of Sustainable Energy Material Chemistry, Xi'an Jiaotong University, Xi'an 710049, PR China.

***E-mail:** wwei.mc@mail.xjtu.edu.cn

ORCID: 0000-0002-8357-8427

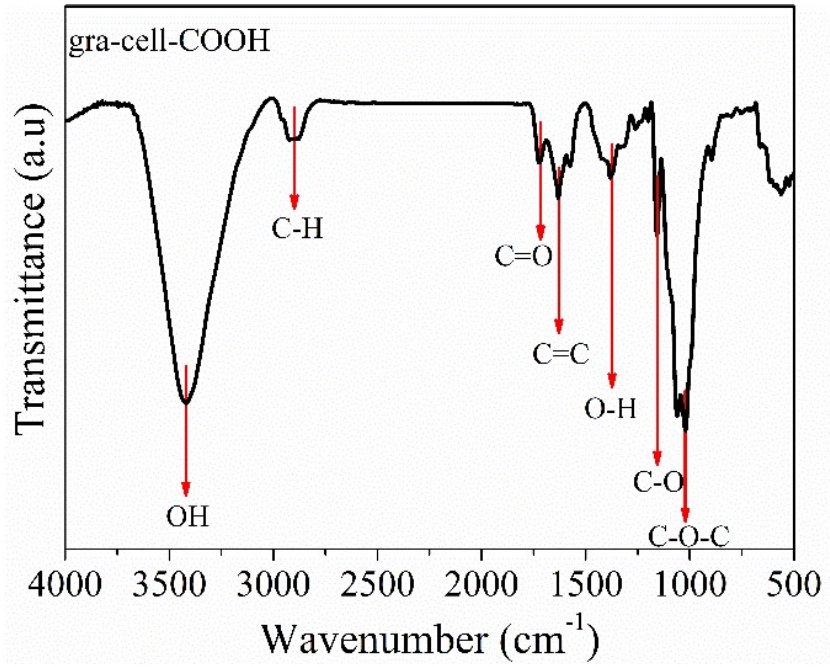

Figure S1 FTIR spectrum of gra-cell-COOH. The absorbance peaks at 1021, 1167, 1387, 2900 and 3435 cm^{-1} stem from celluloses, corresponding to the C–O–C pyranose ring skeletal vibration, C–O antisymmetric stretching vibration in ester, O–H deformation, H–O–H bending of the absorbed water, aliphatic C–H stretching vibrations and stretching of –OH, respectively.

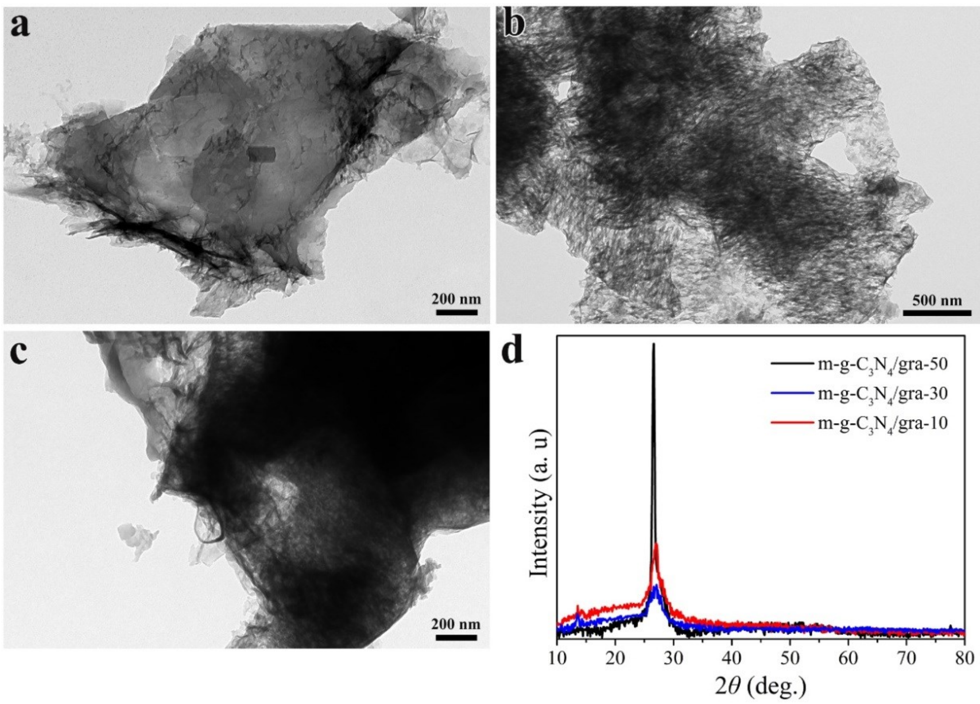

Figure S2 TEM images of (a) m-g-C_3N_4/gra-50, (b) m-g-C_3N_4-30 and (c) m-g-C_3N_4-10; (d) XRD patterns of m-g-C_3N_4/gra-50, m-g-C_3N_4-30 and m-g-C_3N_4-10.

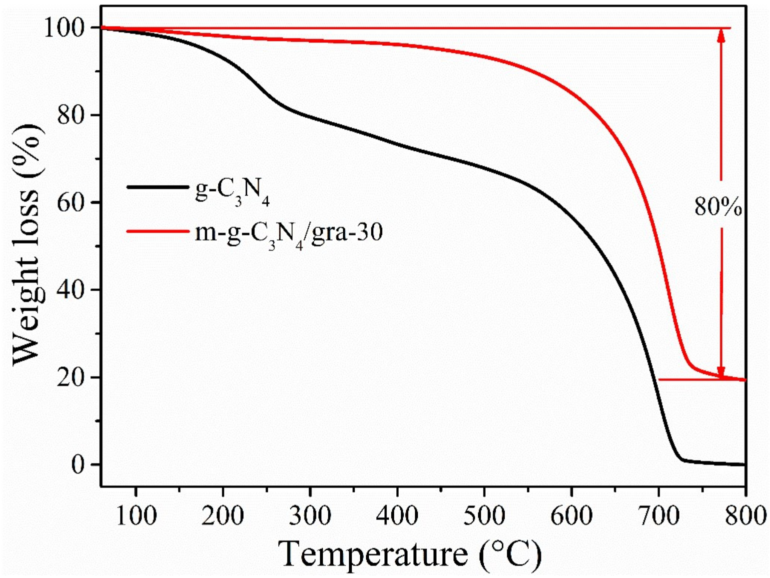

Figure S3 TG curves of g-C_3N_4 and m-g-C_3N_4/gra-30 samples tested under N_2 atmosphere. The g-C_3N_4 decomposed completely at temperatures up to 800 °C while the weight of graphene kept constant under the same condition[1]. The residual mass ratio in the m-g-C_3N_4/gra-30 composites at 800°C is related to the weight ratio of graphene in the composites. Hence, the weight ratio of graphene in m-g-C_3N_4/gra-30 composites is ~20%.

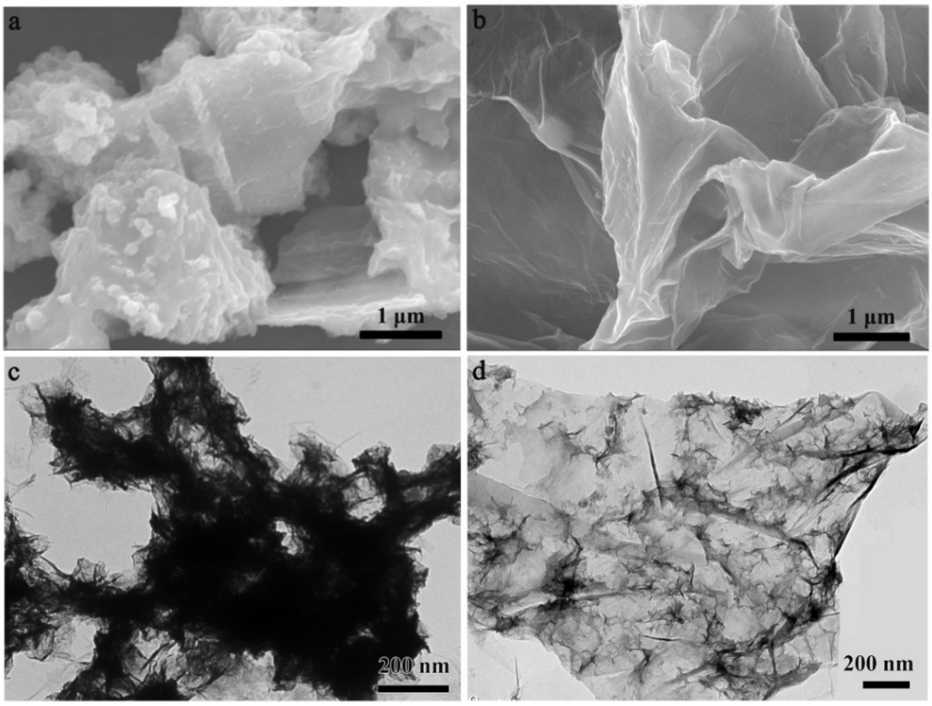

Figure S4 SEM images of (a) pure NiS_2 and (b) NiS_2/gra, TEM image of (c) pure NiS_2 and (d) NiS_2/gra.

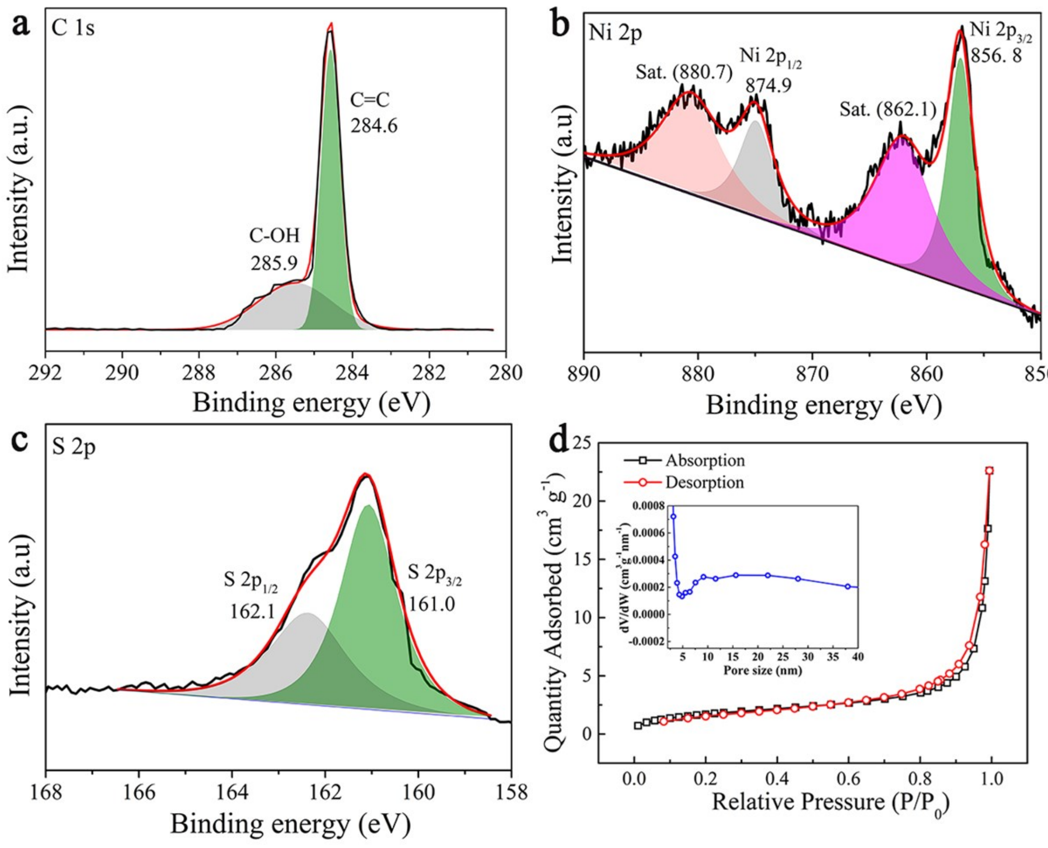

Figure S5 XPS spectra of C1s (a), Ni 2p (b) and S 2p (c) in NiS_2/gra, N_2 adsorption-desorption isotherms (d) of NiS_2/gra (inset: pore-size distribution).

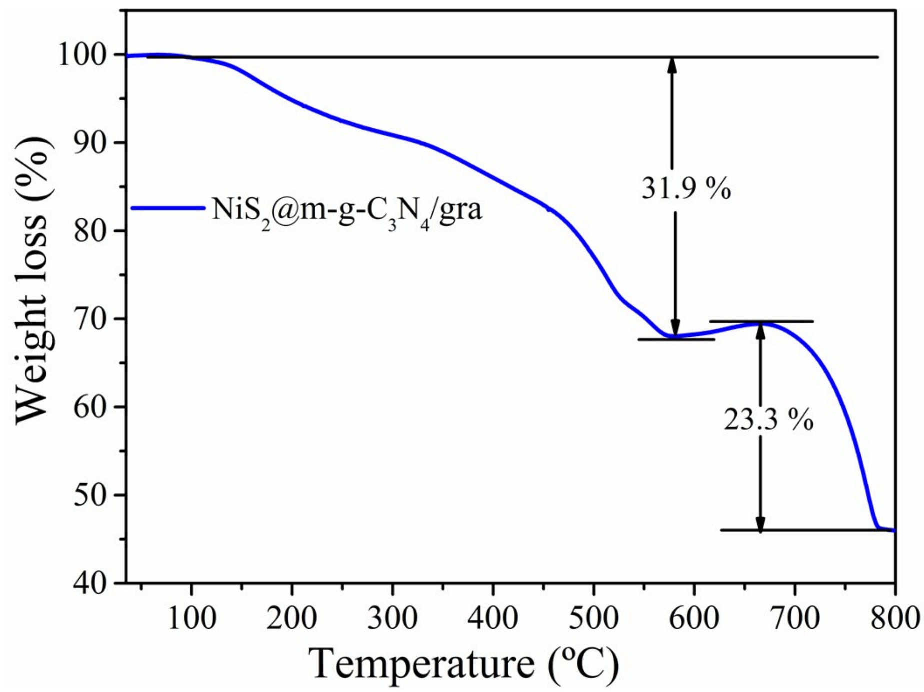

Figure S6 TG curve of NiS_2@m-g-C_3N_4/gra tested under air condition.

To evaluate the content of NiS_2 component in the NiS_2@m-g-C_3N_4/gra, TG analysis is carried out in air atmosphere. A major weight loss of 31.9 wt.% below 580 °C is duo to the burning of m-g-C_3N_4/gra and decomposition of NiS_2 to NiS[2]. Subsequently, the weight was faintly increased within the temperature range from 580 °C to 680 °C stage, which might be ascribed to the transformation of NiS to $NiSO_4$[3]. The final mass loss of 23.3 wt.% within the range of 680-780 °C could be ascribed to the decomposition of $NiSO_4$ to NiO. Based on these results, the reactions of NiS_2 and O_2 during calcination can be proposed as following:

$$NiS_2 + O_2 = NiS + SO_2\uparrow \quad (1)$$

$$2NiS + 3O_2 = 2NiO + 2SO_2\uparrow \quad (2)$$

$$NiO + SO_2 + \frac{1}{2}O_2 = NiSO_4 \quad (3)$$

$$NiSO_4 = NiO + SO_3\uparrow \quad (4)$$

Therefore, the content of NiS_2 component can be calculated from the resitual mass after heating the NiS_2@m-g-C_3N_4/gra composites above 780°C, which is close to 75.7 wt.%.

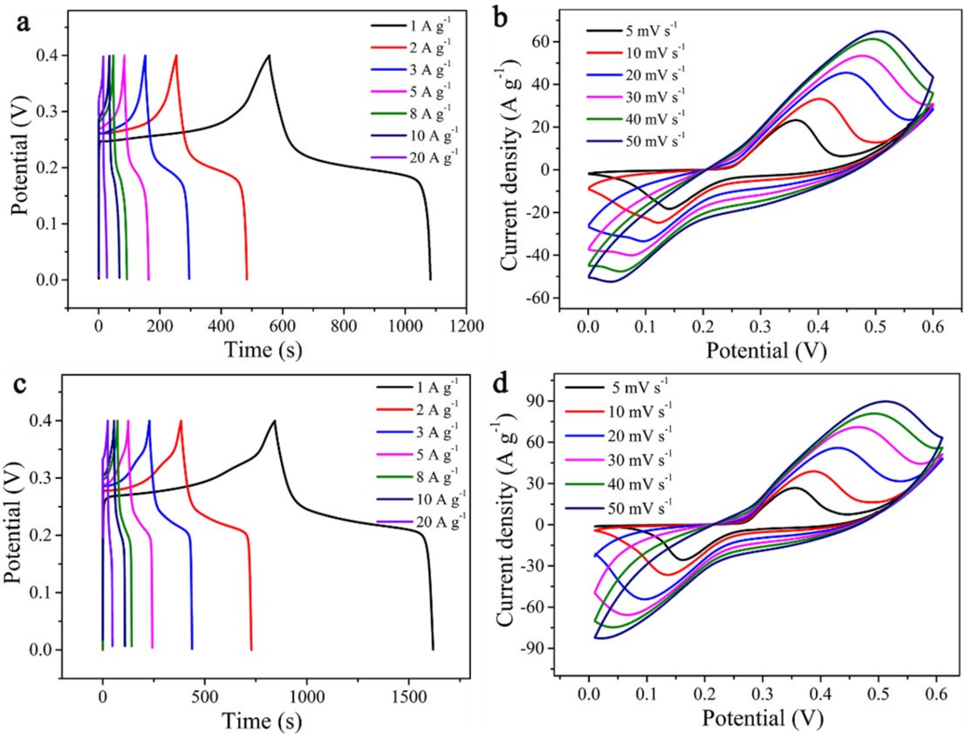

Figure S7 GCD curves of (a) pure NiS_2 and (c) NiS_2/gra electrode; CV curves of (b) pure NiS_2

and (d) NiS_2/gra electrode.

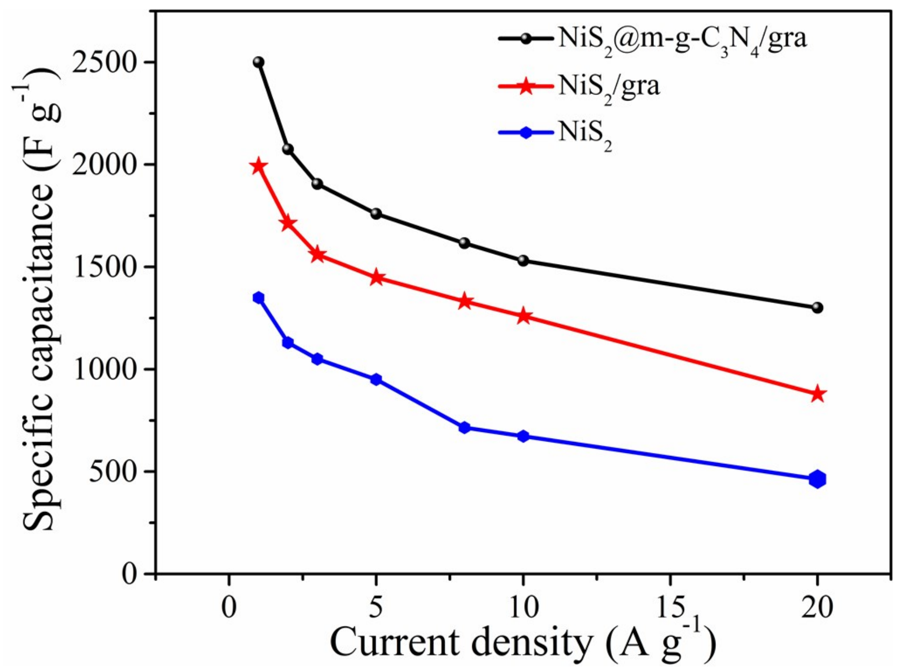

Figure S8 Comparison of specific capacitance of three electrodes at current densities from 1 to 20 A g^{-1}.

Table S1 The specific capacity/capacitance of the NiS_2, NiS_2/gra and NiS_2@m-g-C_3N_4/gra electrodes at various current densities (A g^{-1}).

Current density (A g^{-1})	Specific capacity (mAh g^{-1}) / capacitance (F g^{-1})		
	NiS_2@m-g-C_3N_4/gra	NiS_2/gra	NiS_2
1	296 / 2500	234 / 1991	154 / 1350
2	244 / 2075	208/ 1712	132 / 1130
3	234 / 1905	190/ 1560	121 / 1050
5	200 / 1759	175 / 1448	105 / 950
8	176 / 1616	159 / 1332	86 / 715
10	164 / 1530	149/ 1260	78 / 673
20	150 / 1300	112 / 878	45 / 463

Table S2 Comparison of electrochemical performance of recently reported TMDs/graphene heterostructured electrodes for SC applications.

Electrode	Specific capacitance/capacity	Electrolyte	Ref.
α-NiS/rGO	744 C g^{-1} (1 A g^{-1})	2 M KOH	4
ANM-NiS-rGO	150 mAh g^{-1} (1 A g^{-1})	3 M KOH	5
VS_4/rGO/CoS_2@Co	274.3 mAh g^{-1}(0.625 A g^{-1})	2 M KOH	6
0.5 cP/rGO/Co_9S_8	788.9 (1 A g^{-1})	2M KOH	7
Ni_3S_4@rGO-20	1830 (2 A g^{-1})	2 M KOH	8
MoS_2/3D graphene	102.46 (0.5 A g^{-1})	1 M KOH	9
MoS_2@3DGN	315.6 (1 A g^{-1})	3 M KOH	10
MnS@rGO/Ni-foam	2220 (0.5 A g^{-1})	3 M KOH	11
NiS_2@m-g-C_3N_4/gra	296 mAh g^{-1}/2500 F g^{-1} (1 A g^{-1})	2 M KOH	This work

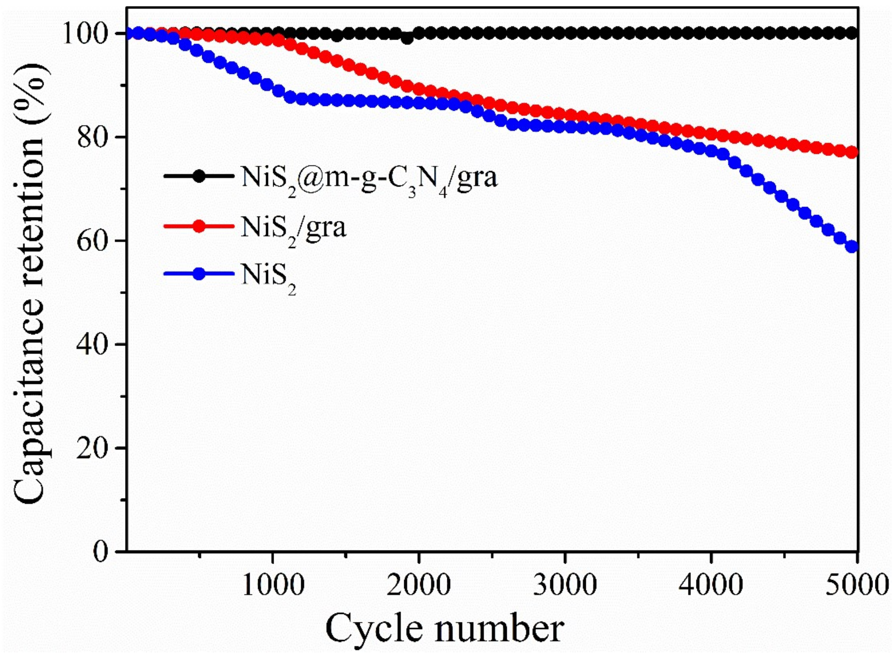

Figure S9 Cycle performances of NiS_2@m-g-C_3N_4/gra, NiS_2/gra and NiS_2 electrodes tested at 5 A g^{-1}.

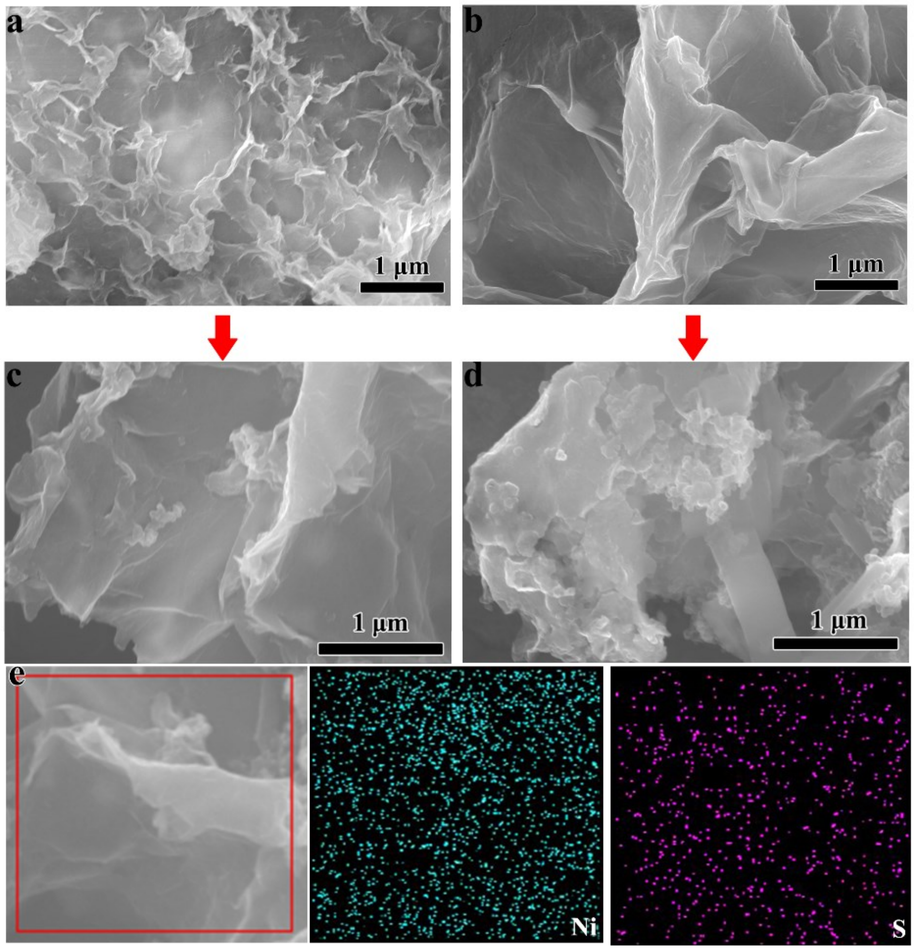

Figure S10 SEM pictures of NiS_2@m-g-C_3N_4/gra electrode before (a) and after cycling test (c), SEM pictures of NiS_2/gra electrode before (b) and after cycling test (d), (e) elemental mapping characterizations for Ni and S of NiS_2@m-g-C_3N_4/gra after cycling.

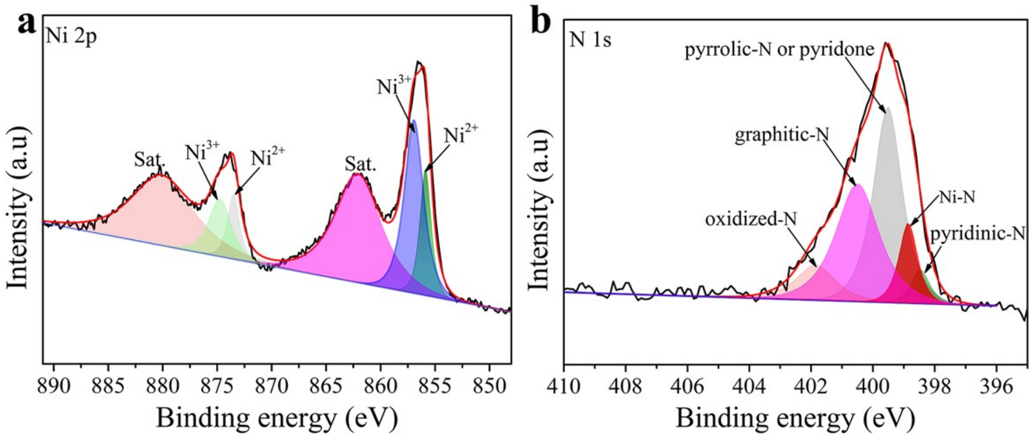

Figure S11 XPS spectrum of Ni 2p (a) and N 1s (b) of NiS_2@m-g-C_3N_4/gra hybrids after cycling test.

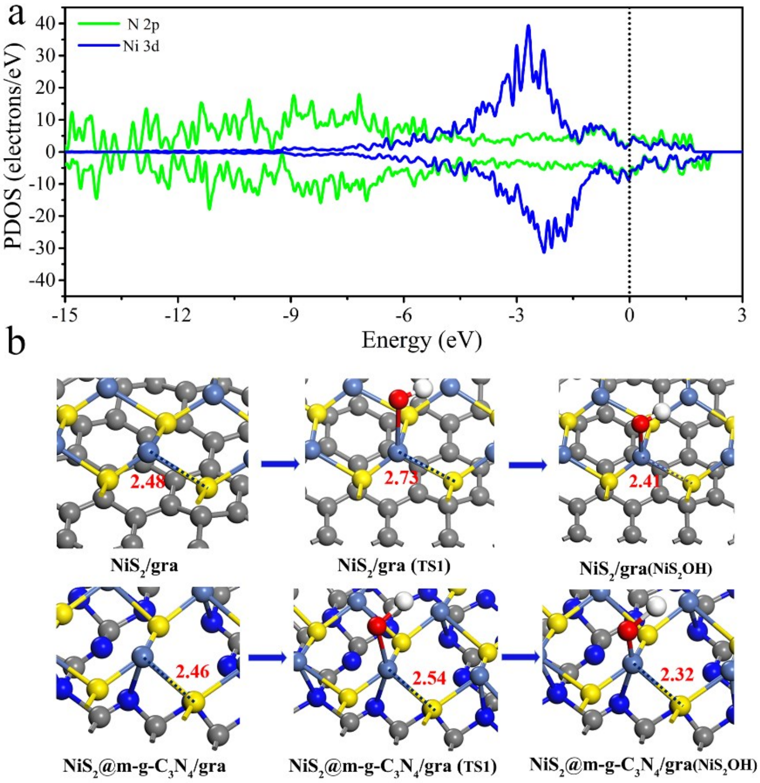

Figure S12 (a) Partial density of states per eV for the nitrogen 2p orbital and nickel 3d orbital in NiS_2@m-g-C_3N_4/gra, and change in Ni-S bond length (b) of NiS_2@m-g-C_3N_4/gra and NiS_2/gra during electrochemical reaction.

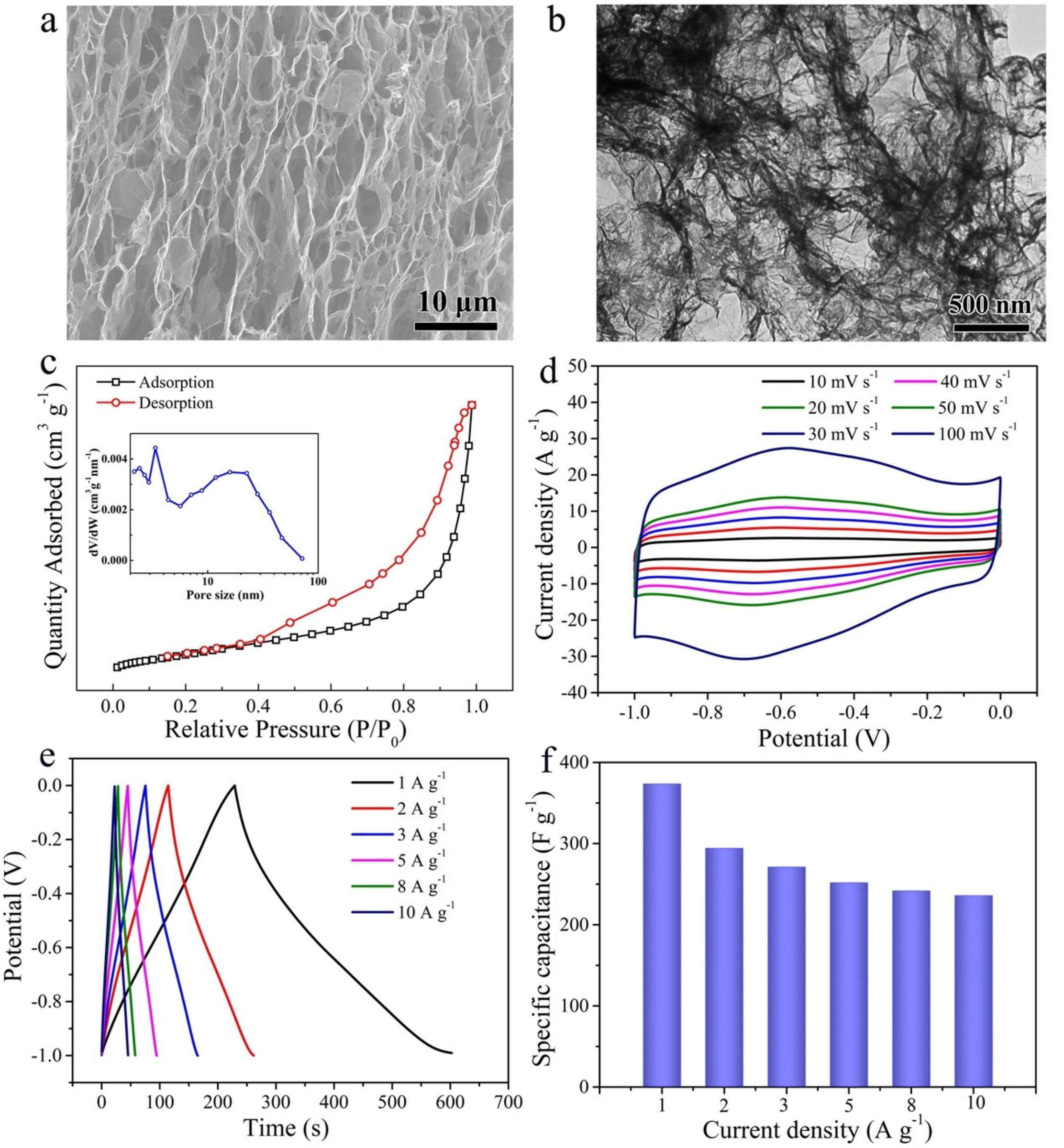

Figure S13 SEM image (a) and TEM image (b) of g-C_3N_4/RGO, N_2 adsorption-desorption isotherms (c) of g-C_3N_4/RGO (inset: pore-size distribution), electrochemical performance of CV curves (d) and GCD curves (e) of g-C_3N_4/RGO, the specific capacitances (f) of g-C_3N_4/RGO at different current densities.

Table S3 Performance comparison of NiS_2@m-g-C_3N_4/gra//RGO/g-C_3N_4 and various HSC devices based on heterostructured hybrids as cathode

Devices	Energy density (Wh kg^{-1})	Power density (W kg^{-1})	Cycle life and capacitance retention	Ref.
0.5 cP/rGO/Co_9S_8//AC	50.3	415.8	8000 cycles (96%)	7
Ni_3S_4@rGO-20//RGO	37.3	398	10000 cycles (91.4%)	8
MoS_2@3DGN //AC	36.43	400	4000 cycles (100%)	10
NiS_2@MoS_2//AC	37.2	800	10000 cycles (80.5%)	12
$NiMn_2O_4$@CoS//SCG	44.56	700	5000 cycles (94.0%)	13
MoS_2/NiS //AC	38.6	400	10000 cycles (100%)	14
NiS_2@m-g-C_3N_4/gra //RGO/g-C_3N_4	63.0	931.2	10000 cycles (100%)	This work

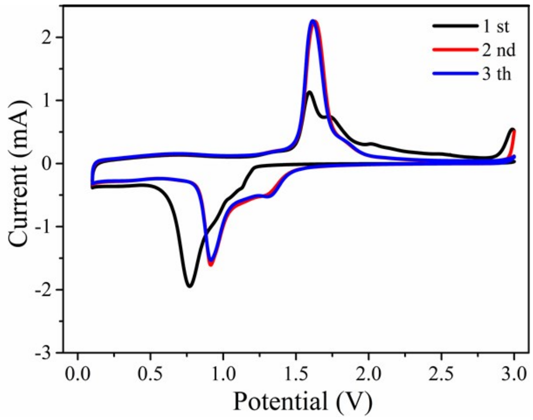

Figure S14 CV curves the NiS_2@m-g-C_3N_4/gra electrode at a scan rate of 0.5 mV s^{-1} with a voltage range of 0.1-3.0 V versus Na^+/Na.

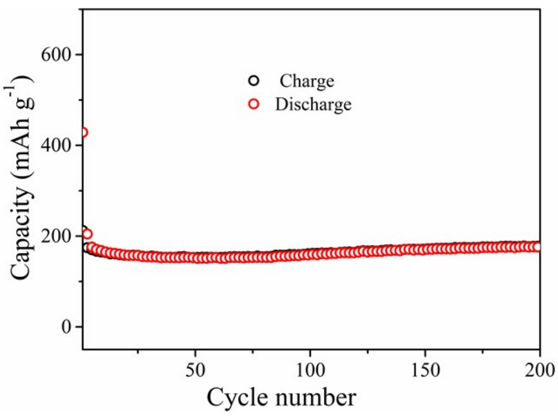

Figure S15 Cycling performance of m-g-C_3N_4/gra at a current density of 0.1 A g^{-1}.

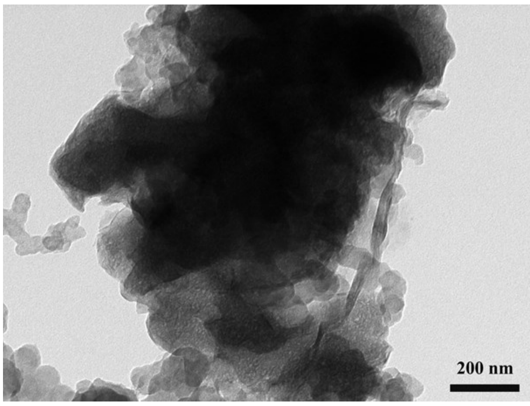

Figure S16 TEM image of NiS_2@m-g-C_3N_4/gra electrode after SIBs test at 2 A g^{-1} for 100 cycles.

References

1. J. Phiri, L.-S. Johansson, P. Gane and T. Maloney, *Compos. Part. B-Eng.*, 2018, **147**, 104-113.
2. S.-L. Yang, H.-B. Yao, M.-R. Gao and S.-H. Yu, *CrystEngComm*, 2009, **11**, 1383-1390.
3. J. Yang, X. Duan, W. Guo, D. Li, H. Zhang and W. Zheng, *Nano Energy*, 2014, **5**, 74-81.
4. C. Qu, L. Zhang, W. Meng, Z. Liang, B. Zhu, D. Dang, S. Dai, B. Zhao, H. Tabassum, S. Gao, H. Zhang, W. Guo, R. Zhao, X. Huang, M. Liu and R. Zou, *J. Mater. Chem. A*, 2018, **6**, 4003-4012.
5. T. C. Ke, B. Vedhanarayanan, L. D. Shao and T. W. Lin, *ChemElectroChem*, 2019, **6**, 3806-3814.
6. S. Wang, Y. Song, Y. Ma, Z. Zhu, C. Zhao and C. Zhao, *Chem. Eng. J.*, 2019, **365**, 88-98.
7. T. Yao, Y. Li, D. Liu, Y. Gu, S. Qin, X. Guo, H. Guo, Y. Ding, Q. Liu, Q. Chen, J. Li and D. He, *J. Power Sources*, 2018, **379**, 167-173.
8. Q. Hu, X. Zou, Y. Huang, Y. Wei, YaWang, F. Chen, B. Xiang, Q. Wu and W. Li, *J. Colloid Interface Sci.*, 2020, **559**, 115-123.
9. B. Xie, Y. Chen, M. Yu, S. Zhang, L. Lu, Z. Shu and Y. Zhang, *RSC Adv.*, 2016, **6**, 89397-89406.
10. R. Zhou, C.-j. Han and X.-m. Wang, *J. Power Sources*, 2017, **352**, 99-110.
11. P. Naveenkumar and G. Paruthimal Kalaignan, *Electrochim. Acta*, 2018, **289**, 437-447.
12. S. Hou, Y. Lian, Z. Xu, D. Wang, C. Ban, J. Zhao and H. Zhang, *Electrochim. Acta*, 2020, **330**, 135208-135210.
13. N. Hu, L. Huang, W. Gong and P. K. Shen, *ACS Sustain. Chem. Eng.*, 2018, **6**, 16933-16940.
14. Q. Qin, L. Chen, T. Wei and X. Liu, *Small*, 2019, **15**, 1803639-1803613.